

# Simulation study of an auto-thermal double-membrane reactor for the simultaneous production of hydrogen and methanol: comparison of two different hydrogen redistribution strategies along the reactor

Farhad Rahmani<sup>1, 2</sup>, Mohammad Haghghi<sup>1, 2\*</sup>, Pooya Estifaei<sup>1, 2</sup>, Mohammad Reza Rahimpour<sup>3</sup>

<sup>1</sup>Sahand University of Technology, Chemical Engineering Faculty, P.O.Box 51335-1996, Sahand New Town, Tabriz, Iran

<sup>2</sup>Sahand University of Technology, Reactor and Catalysis Research Center (RCRC), P.O.Box 51335-1996, Sahand New Town, Tabriz, Iran

<sup>3</sup>Shiraz University, Chemical Engineering Department, School of Chemical and Petroleum Engineering, Shiraz, Iran

\*corresponding author: e-mail: haghghi@sut.ac.ir

In a continuing effort to realize the simultaneous hydrogen and methanol production via the auto-thermal methanol synthesis process, the effect of two different hydrogen redistribution strategies along a double-membrane reactor has been considered. A steady-state one-dimensional heterogeneous model was developed to compare two strategies applied in the operation of the auto-thermal methanol synthesis. It was found that the counter-current configuration exhibited the better performance compared to the reactor operated in the co-current mode from both the economic and environmental points of view. This superiority is ascribed to the establishment of a more favourable temperature profile along the reactor and also more hydrogen extraction from the reaction zone. Moreover, the influence of some operating variables was investigated on the performance of the auto-thermal double-membrane reactor in the counter-current configuration. The results suggest that utilizing this configuration for pure hydrogen and methanol production could be feasible and beneficial.

**Keywords:** pure hydrogen production, methanol synthesis, auto-thermal double-membrane reactor, steady-state heterogeneous model, operation mode.

## INTRODUCTION

At present, the energy resources are mainly based on fossil fuels which are absolutely essential for the prosperity of mankind. Concerns about the environmental misdeeds of fossil fuels and also the growing gap between increasing demand and shrinking supply as a result of the continuous increase in the global population and economic development, and the rapid depletion of fossil fuels, respectively, have led to significant research into the use of alternative energy carriers. Hydrogen and methanol have been identified as ideal energy carriers to support sustainable energy development<sup>1–4</sup>. Widespread usage of them, if generated in an advantageous manner, could contribute to alleviation of the growing concerns about the world's energy supply, security, air pollution and greenhouse gas emissions<sup>5</sup>. Although hydrogen is often referred to as 'clean energy' since its combustion produces only water while the production of hydrogen from hydrocarbons via conventional processes, yields CO<sub>2</sub>, a greenhouse gas. Therefore, one of the environmentally benign methods to produce hydrogen without CO<sub>2</sub>-emission is cyclohexane dehydrogenation<sup>6–8</sup>. Commercially, methanol, on the other hand, is produced by the natural gas and specifically by means of syngas obtained via steam reforming operations<sup>9–12</sup>.

Currently, some alternative processes such as auto-thermal methanol synthesis (AMS) are considered to co-produce hydrogen and methanol as environment friendly fuel<sup>13–16</sup>. Indeed, AMS combines methanol synthesis and cyclohexane dehydrogenation reactions in a single reactor. However, the AMS process is affected by the thermodynamic constraints, which limit reactants conversion. Under such circumstances, using the membrane concept in the auto-thermal methanol process seems to be beneficial in order to selectively in situ product removal or reactant addition. Pd-Ag membranes have attracted increasing attention in membrane reactors in

the hydrogen production and methanol synthesis processes. On this base, promising candidates in the auto-thermal methanol synthesis process are double-Pd/Ag membrane and two-membrane fixed-bed reactors, which have proposed by Rahimpour et al.<sup>17–18</sup>. These reactor configurations consist of two catalytic fixed beds separated by the tube wall and also two membranes, one (Pd/Ag membrane) is used for pure hydrogen production from the endothermic side and the subsequent is employed in order to selectively in-situ hydrogen addition to the exothermic side via another Pd/Ag membrane (in the case of the double-Pd/Ag membrane configuration reactor) or selectively in-situ water removal from the exothermic side by means of H-SOD membrane (in the case of the two-membrane configuration reactor). The results of their investigation obtained in distinct studies revealed that the mentioned reactors in addition to possessing advantages of an auto-thermal membrane methanol synthesis reactor (AMMSR), have more favourable temperature profile and higher productivity. However, glancing over their results shows that although lower production rate of water in the thermally coupled two-membrane reactor (TCTMR) reduces catalyst re-crystallization, the auto-thermal double-membrane reactor (ADMR) has superiority over the TCTMR due to higher production and conversion. In addition, it is interesting to highlight that it was not easy to synthesize this type of membrane, so this could count as a disadvantage. In this regard, it was decided to peruse more study on ADMR.

The reported literatures reflect that the majority of the implemented works on the coupled reactors have reported higher conversion and performance in the co-current mode of reacting gas mixtures in both the exothermic and endothermic sides. Therefore, in the utilization of an ADMR, the important parameters to be taken into accounts are the relative direction of both the synthesis gas and recycle streams in the exothermic and recycle

sides, respectively. In particular, there are differences in terms of both hydrogen recovery yield and methanol production when the co-current mode or the counter-current one is used. The use of the counter-current mode was already studied from a theoretical point of view in reaction systems such as methane steam reforming<sup>19</sup>, methanol steam reforming<sup>20–21</sup> and water gas-shift reaction<sup>22</sup>, carried out in Pd–Ag membrane reactors. These studies found that the counter-current modes able to increase the hydrogen recovery with respect to the co-current one for a wide range of operative conditions. Differences between the performances of membrane reactor operated in the co-current and counter-current modes have also been observed for other reaction systems<sup>23–24</sup>.

The positive effect of the counter-current mode on reactor performance and failure in finding research dealing with comparison of the two operation mode effect on ADMR performance persuade us to investigate the performance of two ADMR configurations which is the subject of the present work, would be beneficial and helps policy makers to identify the promising configuration and technology. In the present work, the effect of hydrogen redistribution along an auto-thermal double-membrane reactor was studied. In the first strategy, hydrogen permeates into the exothermic side in the co-current operation mode while in the second strategy, it happens in the counter-current one. Consequently, a steady-state 1-D mathematical model has been used for the simulation of this reactor operated in both the co-current and counter-current modes. The performances in terms of methanol production, cyclohexane conversion and hydrogen recovery of both the configurations have been compared at same process conditions such as pressure, temperature, catalyst mass and feed composition.

## PROCESS DESCRIPTION

### Auto-thermal double-membrane reactor (TCDMR)

Figure 1 shows the schematic flow diagram of an auto-thermal double-membrane reactor for simultaneous pure hydrogen and methanol production in the counter-current configuration, respectively. ADMR consists of four concentric tubes. The inner tube is the recycle side which is separated by a Pd–Ag membrane from the exothermic side (second tube). The catalytic dehydrogenation of cyclohexane to benzene is assumed to take place in the third side while the methanol synthesis occurs inside the next compartment. Synthesis gas is fed to the exothermic side and its effluent is recycled, compressed (up to 96.98 bar) and passed through the inner tube in a co-current mode<sup>18</sup> or counter-current mode (see Fig. 1) with respect to reacting gas. Hydrogen partial pressure in the recycle stream (after it was compressed) is suitable for hydrogen permeation into the exothermic side. After leaving the inner tube (the recycle side), the methanol rich-gas (product stream) goes to the separator. Therefore, the exothermic stream is cooled simultaneously with the recycling gas in the inner tube and the reacting gas in the endothermic side. Moreover, pure hydrogen is produced via the membrane wall in the latter section and is swept by an inert gas. The input data and operating conditions are available in our previous reports<sup>14, 18, 25–26</sup>.

## REACTION SCHEME AND KINETICS

### Methanol synthesis

In the methanol synthesis, three overall reactions are possible: hydrogenation of carbon monoxide, hydrogenation of carbon dioxide and reverse water–gas shift reactions:

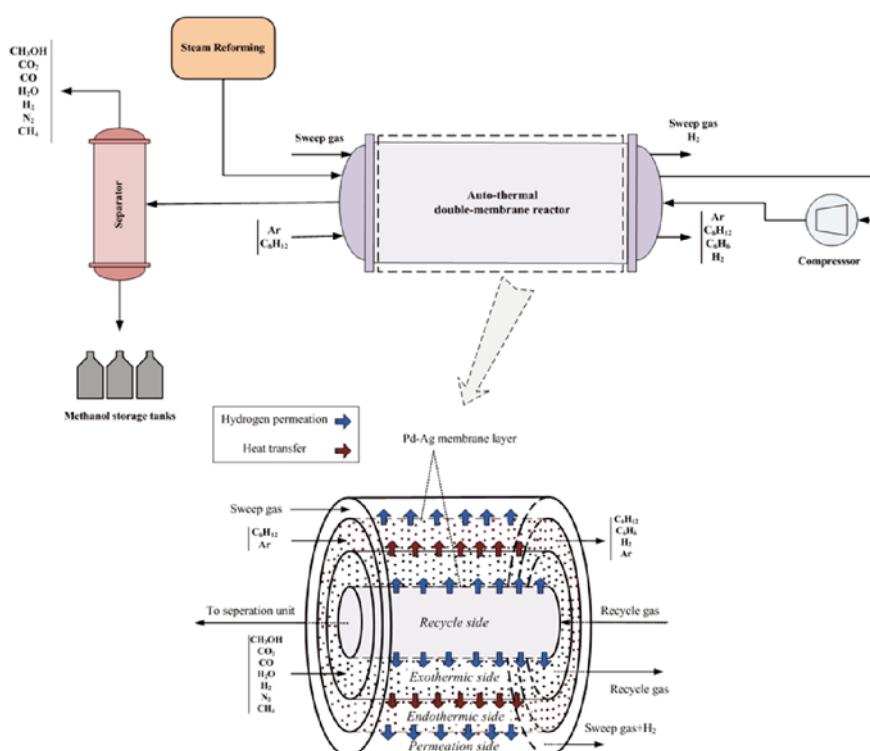
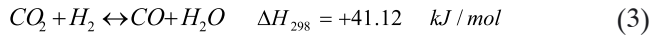
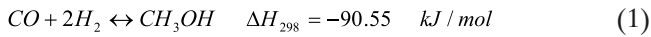


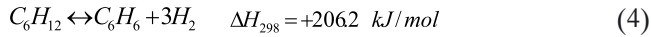
Figure 1. Schematic diagram of ADMR in the counter-current mode



In the current work, the rate expressions have been selected from Graaf et al.<sup>27</sup>. The rate equations combined with the equilibrium rate constants<sup>28</sup> provide enough information about the kinetics of the methanol synthesis over commercial CuO/ZnO/Al<sub>2</sub>O<sub>3</sub> catalysts.

### Dehydrogenation of Cyclohexane

The reaction scheme for the dehydrogenation of cyclohexane to benzene is as follows:



The following reaction rate equation of cyclohexane,  $r_c$ , is used<sup>29</sup>:

$$r_c = \frac{-k(K_p P_C / P_{H_2}^3 - P_B)}{1 + (K_B K_p P_C / P_{H_2}^3)} \quad (5)$$

where  $k$ ,  $K_B$  and  $K_p$  are the reaction rate constant, the adsorption equilibrium constant for benzene and the reaction equilibrium constant, respectively. Moreover,  $P_i$  is the partial pressure of component  $i$  in Pa. The reaction temperature is in the range of 423–523 K and the total pressure in the reactor is maintained at 101.3 kPa. The catalyst is Pt/Al<sub>2</sub>O<sub>3</sub><sup>30</sup>.

### MATHEMATICAL MODELLING

The following assumptions were considered for modelling the double- and single-membrane heat exchanger reactors:

- One-dimensional heterogeneous model (reactions take place on the catalyst surface);
- Steady state operation;
- Plug flow pattern in each sides;
- Axial diffusion of heat and mass are negligible;
- No radial diffusion of heat and mass in the catalyst pellets;
- Catalytic beds have symmetry (bed porosity in axial and radial directions is constant);
- Ideal gas behaviour on each sides;
- Outer wall is considered to be insulated.

According to the above mentioned assumptions and the differential element along the axial direction inside the reactor, the mole and energy balance equations were obtained. The balances typically account for the convection, transport to the solid-phase and reaction. The mass and energy balances, pressure drop equation and boundary conditions for solid and fluid phases have been summarized in Table 1. In equations (6) and (7),  $\eta$  is effectiveness factor of  $k^{th}$  reaction in  $j^{th}$  side (the ratio of the reaction rate observed to the real rate of

**Table 1.** The mass and energy balances and the boundary conditions for the solid and fluid phases in different sides of ADMR

	Mass and energy balances equation	Number
	$a_v c_j k_{g,i,j} (y_{i,j}^g - y_{i,j}^s) + \eta r_{i,j} \rho_b = 0$	(6)
Solid phase	$a_v h_f (T_j^g - T_j^s) + \rho_b \sum_{i=1}^N \eta r_{i,j} (-\Delta H_{f,i}) = 0$	(7)
	$-\frac{F_j}{A_{c,j}} \frac{dy_{i,j}^g}{dz} + a_v c_j k_{g,i,j} (y_{i,j}^s - y_{i,j}^g) - \beta \frac{J_{H_3}}{A_{c,j}} + \phi \frac{J_{H_1}}{A_{c,j}} = 0$	(8)
Fluid phase	$-\frac{F_j}{A_{c,j}} C_{p,j}^g \frac{dT_j^g}{dz} + a_v h_f (T_j^s - T_j^g) \pm \frac{\pi D_i}{A_{c,j}} U (T_3^g - T_2^g) - \beta \frac{J_{H_3}}{A_{c,j}} \int_{T_3}^{T_4} C_p dT$ $- \beta \frac{\pi D_i}{A_{c,j}} U_{3-4} (T_3^g - T_4^g) + \phi \frac{\pi D_i}{A_{c,j}} U_{1-2} (T_1^g - T_2^g) + \phi \frac{J_{H_1}}{A_{c,j}} \int_{T_1}^{T_2} C_p dT = 0$	(9)
Permeation side	$-F_4 \frac{dy_{i,4}^g}{dz} + \beta J_{H_3} = 0$	(10)
	$-F_4 C_{p,4}^g \frac{dT_4^g}{dz} + \beta J_{H_3} \int_{T_3}^{T_4} C_p dT + \pi D_i U_{3-4} (T_3^g - T_4^g) = 0$	(11)
Recycle side	$\pm F_1 \frac{dy_{i,1}^g}{dz} - \phi J_{H_1} = 0$	(12)
	$\pm F_1 C_{p,1}^g \frac{dT_1^g}{dz} - \phi J_{H_1} \int_{T_1}^{T_2} C_p dT + \pi D_i U_{1-2} (T_2^g - T_1^g) = 0$	(13)
The initial value	$z = 0 \quad y_{i,j}^g = y_{i0,j}^g, T_j^g = T_0^g, P_j^g = P_0^g \quad j=2, 3, 4$	(14)
Co-current	$z = 0 \quad y_{i,1}^g = y_{if,2}^g, T_1^g = T_{f,2}^g, P_1^g = P_{f,2}^g \quad j=1$	(15)
Counter-current	$z = L \quad y_{i,1}^g = y_{if,2}^g, T_1^g = T_{f,2}^g, P_1^g = P_{f,2}^g \quad j=1$	(16)

reaction), which is obtained from the dusty gas model<sup>26</sup>. In equations (8) and (9),  $\beta$  and  $\phi$  are equal to 1 and 0 for the endothermic and 0 and 1 for the exothermic side, respectively. Besides, in equation (9), the positive and negative signs are used for exothermic and endothermic sides, respectively. In equations (10) and (11),  $\beta$  is equal to 1 for hydrogen component and 0 for the sweep gas. The negative and positive signs of the first term in equations (12) and (13) are used for the co-current and the counter-current flow, respectively. Moreover, in equations (12) and (13),  $\phi$  is equal to 1 for hydrogen component and 0 for CO<sub>2</sub>, CO, H<sub>2</sub>O, CH<sub>3</sub>OH and inert components. In the boundary condition equations,  $y_{i0,j}^g$ ,  $T_0^g$  and  $P_0^g$  are the mole fraction of  $i^{\text{th}}$  component in the fluid-phase, temperature and pressure at the entrance of  $j^{\text{th}}$  side of the reactor, respectively.  $y_{if,2}^g$ ,  $T_{f,2}^g$  and  $P_{f,2}^g$  are the mole fraction of  $i^{\text{th}}$  component in the fluid-phase, temperature and pressure at the end of the exothermic side, respectively.

### Auxiliary correlations

In order to simulate the reactor and solve the set of differential equations, auxiliary correlations should be added. The Ergun momentum balance equation is used to give the pressure drop along the reactor. Moreover, the flux of hydrogen permeating through the inner and outer Pd/Ag membranes is assumed to follow the half-power pressure law (Sievert's law) expressed by:

$$J_{H_2} = \frac{2\pi L \bar{P}_0}{\ln\left(\frac{D_o}{D_i}\right)} \exp\left(\frac{-E_p}{RT}\right) (\sqrt{P_{H_2,1}} - \sqrt{P_{H_2,2}}) \quad (17)$$

$$J_{H_2} = \frac{2\pi L \bar{P}_0}{\ln\left(\frac{D_o}{D_i}\right)} \exp\left(\frac{-E_p}{RT}\right) (\sqrt{P_{H_2,3}} - \sqrt{P_{H_2,4}}) \quad (18)$$

$P_{H_2}$  is hydrogen partial pressure in Pa.  $D_o$  and  $D_i$  stand for the outer and inner diameters of the Pd/Ag layer. The pre-exponential factor  $\bar{P}_0$  above 200°C is reported as  $6.3 \times 10^{-8} \text{ molm}^{-2}\text{s}^{-1}\text{Pa}^{-0.5}$  and the activation energy  $E_p$  is  $15.7 \text{ kJmol}^{-1}$ <sup>18, 31</sup>.

The correlations used for heat and mass transfer between two phases, physical properties of chemical species and overall heat transfer coefficient between two sides were adopted from the literature<sup>32-34</sup>.

### Numerical solution

The governing equations of the model form a system of coupled equations comprising of partial derivative equations of mass and energy conservation rules for the fluid and solid phases; aforementioned correlations for the heat and mass transfer coefficients and the physical properties of fluids; as well as the nonlinear algebraic equations of the kinetic model. After rewriting the model equations, a set of differential algebraic equations (DAEs) is obtained for both the co-current and counter-current modes. This set of equations is changed to nonlinear algebraic equations (NAEs) using the backward finite difference approximation. The NAEs constitute an initial value problem that was solved using the shooting method in the counter-current mode and the trial-and-error method in the co-current mode. The reactor length is then divided into 100 separate sections and the Gauss-Newton method in MATLAB programming

environment is used to solve the non-linear algebraic equations in each section.

### Solution procedure for co-current mode

In the co-current mode, the calculation was started with initial guesses for the inlet temperature ( $T_{\text{in}}$ ) and hydrogen mole fraction ( $y_{\text{in}}$ ) of the effluent synthesis gas fed to the recycle gas side, which are unknown (initial conditions). The initial conditions were calculated using the Gauss-Newton method corrected by the previous values of temperature and hydrogen mole fraction of the synthesis gas in the exothermic side outlet in subsequent calculations. Substitution was continued until the convergence criterion was met.

### Solution procedure for counter-current mode

In the counter-current mode, the inlet temperature ( $T_{\text{in}}$ ) and hydrogen mole fraction ( $y_{\text{in}}$ ) of the effluent synthesis gas fed to the recycle side are unknown (final conditions). Solution is possible by guessing values for  $T_{\text{out}}$  and  $y_{\text{out}}$  of the recycle gas leaving the inner tube. Then, the Gauss-Newton method was used to solve the nonlinear algebraic equations in each node. In the end, the calculated values of temperature and hydrogen mole fraction of the recycle gas were compared with the calculated values of temperature and hydrogen mole fraction of the synthesis gas in the outlet of the exothermic side. This procedure was repeated until the specified terminal values were obtained within a small convergence criterion.

## RESULTS AND DISCUSSIONS

### Model validation

The applied model was validated against the plant data from the conventional methanol synthesis reactor for a special case of constant coolant temperature under the design specifications. The comparison between the simulation and plant data<sup>35</sup> has been shown in Table 2. The modelling outcomes perform satisfactorily well under special case of industrial conditions and the observed plant data are in good agreement with simulation data.

In this section, various steady-state behaviours observed in the coupled reactors are analyzed and the predicted molar flow rate, yield, conversion and temperature profiles are presented. The performance of the thermally coupled reactor is analyzed, using different operating variables, for methanol yield, cyclohexane conversion and hydrogen recovery yield as follows:

$$\text{Hydrogen recovery yield} = \frac{F_{H_2,3}}{F_{C_6H_{12},in}} \quad (19)$$

$$\text{Methanol yield} = \frac{F_{CH_3OH,out}}{F_{CO,in} + F_{CO_2,in}} \quad (20)$$

$$\text{Cyclohexane conversion} = \frac{F_{C_6H_{12},in} - F_{C_6H_{12},out}}{F_{C_6H_{12},in}} \quad (21)$$

**Table 2.** Comparison between simulation and plant data<sup>35</sup> for the conventional methanol synthesis reactor

	Reactor inlet	Exp.	Reactor outlet	Error [%]
			Calc.	
Composition [mol %]				
CO <sub>2</sub>	3.45	2.18	2.26	-3.67
CO	4.66	1.44	1.5	-4.167
H <sub>2</sub>	79.55	75.71	76.37	-0.87
CH <sub>4</sub>	11.72	12.98	12.88	0.77
N <sub>2</sub>	0.032	0.16	0.15	6.66
H <sub>2</sub> O	0.08	1.74	1.66	4.598
CH <sub>3</sub> OH	0.032	5.49	5.23	4.736
Feed flow rate [mols <sup>-1</sup> ]	0.565	0.51	0.5	1.96
Temperature [K]	503	528	524.3	0.7

## Molar and thermal behaviour comparison

### Exothermic side

Figure 2(a)–(d) demonstrates a comparison of the temperature and molar flow rate profiles of the components along the exothermic side of reactor for the co- and counter-current configurations. Along the exothermic side of the auto-thermal reactors, the temperature increases smoothly and hot spots develop as demonstrated in Figure 3(a) but then decreases. As can be seen in Figure 2(a), the counter-current configuration operates at higher temperature in the first part of the reactor with respect to the co-current one mainly due to lower heat transfer from the exothermic side. Afterwards, the temperature

reduces mainly due to higher heat transfer, as shown in Figure 2(a). Implementing a higher temperature at the entrance of the reactor for a higher reaction rate, and then reducing temperature gradually towards the reactor's outlet for increasing thermodynamic equilibrium conversion is one of the significant issues in the methanol synthesis reactor configuration. Therefore, the most favourable exothermic temperature profile seems that belongs to the counter-current configuration. However, the exothermic temperature control of the co-current configuration is easier due to lower hot spot.

Figure 2(b)–(d) compares the molar flow rate of the components along the exothermic side of the reactor in the co- and counter-current modes. Indeed, these figures represent the effect of recycle gas flow mode in the inner

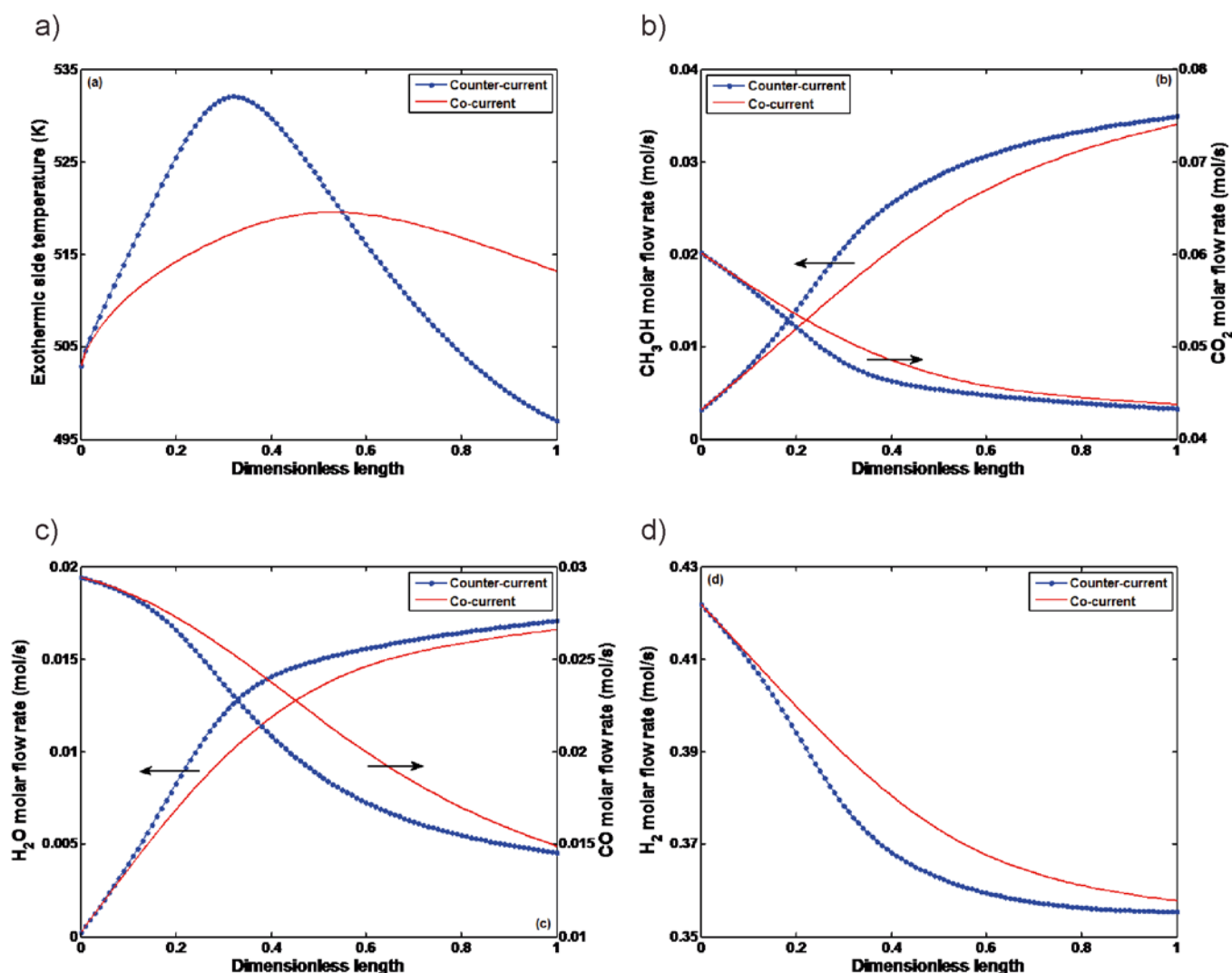


**Figure 2.** Variation of (a) exothermic temperature, (b) methanol and CO<sub>2</sub>, (c) H<sub>2</sub>O and CO; and (d) H<sub>2</sub> molar flow rate along the reactor axis between exothermic sides of the co- and counter-current configurations

tube on the conversion of the exothermic reaction. As can be seen, the molar flow rate of water in the co-current mode is lower than that in the counter-current mode. However, the conversion of carbon oxides and the molar flow rate of methanol in the counter-current mode are higher. Consequently, the counter-current mode is suitable from the point of view of carbon dioxide removal and methanol production, whereas the reactor in the co-current configuration operates with lower water production. Enhancement of the carbon oxides removal in the counter-current mode brings a lower environmental impact. The lower production rate of water in the co-current mode results in the reduction of catalyst re-crystallization and longer catalyst life.

### Endothermic side

Figure 3(a)–(b) illustrates the axial temperature and molar flow rate of the components along the endothermic sides of the auto-thermal configurations. The temperature of the endothermic side is always lower than that of the exothermic side in order to make a driving force for heat transfer from the solid wall. At the entrance of the endothermic side of auto-thermal reactors, the temperature decreases rapidly and a cold spot form and then, the temperature increases (see Fig. 3(a)).

The profiles of components' mole fractions in the thermally coupled reactors are compared in Figure 3(b). According to this comparison, the highest reaction yield

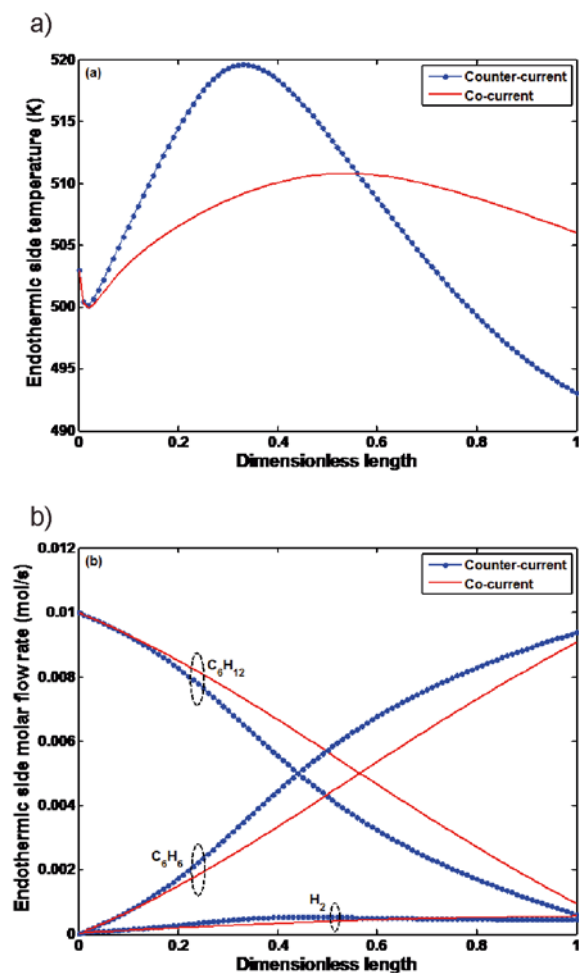


Figure 3. Comparison of (a) temperature, (b) molar flow rate of components along the reactor axis between endothermic sides of the co- and counter-current configurations

is achieved in the counter-current mode and the difference between the co- and counter-current configuration performances is attributed to the high temperature in the early parts of the reactor. Regarding to thermodynamic restrictions and the high endothermicity of cyclohexane dehydrogenation, high temperature results in a higher reaction rate and thereupon, higher conversion. However, the high temperature in the initiation steps of reaction is more important due to high concentrations of the reactants.

### Non-reaction sides

Figure 4(a) and (b) reveal the molar flow rate profile of hydrogen along the reactor axis in the recycle and permeation sides of both configurations, respectively. As can be seen in these figures, the molar flow rate profiles of hydrogen along the reactor length have the same patterns in the permeation side while the trends for the recycle side are completely different. In fact, the molar flow rate of hydrogen in the recycle side diminishes due to the permeation through the inner membrane into the exothermic side while it increases in the permeation side due to delivery of produced hydrogen from the endothermic side via permeation through the outer membrane. As can be seen in Figure 4(b), there is a considerable enhancement in amounts of hydrogen flow rate in the counter-current configuration mainly

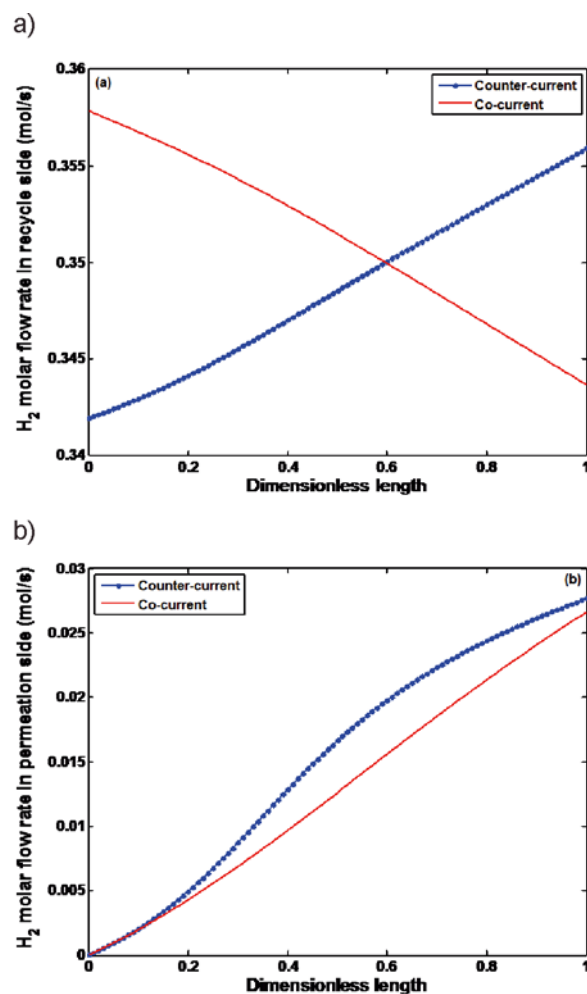


Figure 4. Comparison of H<sub>2</sub> molar flow rate along the reactor axis (a) in the recycle side and (b) in the permeation side of both the configurations

due to higher reaction yield in the endothermic side in comparison to that of the co-current one.

### Production rates

As mentioned previously, the main goal of the auto-thermal process is co-production of useful chemicals that leads to enormous enhancement in the net profit of plant. The methanol, benzene and hydrogen production in each operation mode of TCDMR are presented in Figure 5. As can be seen, the methanol, benzene and pure hydrogen production of the counter-current configuration are 7.02, 6.385 and 0.548 ton day<sup>-1</sup>, respectively, which are higher than the co-current one. This considerable improvement in the chemicals production rate of the counter-current configuration is attributed to the positive effect of counter-current flow pattern of the recycle gas in the inner tube.

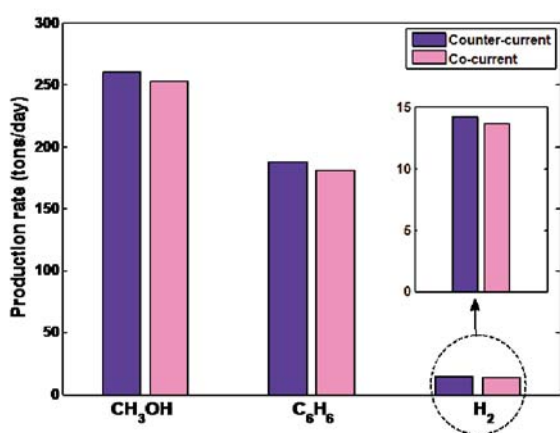


Figure 5. The comparison of methanol, benzene and pure hydrogen production rate in the co- and counter-current operation modes of TCDMR

### Comparison of ADMR Configurations Performance

The performance of TCDMR for the co- and counter-current modes is summarized in Table 3 in terms of feedstock conversion and products yield. Clearly, the counter-current mode has superiority over the co-current one due to higher production and conversion. The effect of counter-current flow pattern is obvious in the performance of TCDMR. The simulation results represent 2.46 and 2.34% enhancement in the methanol yield and synthesis gas conversion in comparison with the co-current configuration, respectively. Besides, the hydrogen recovery yield and cyclohexane conversion (or benzene yield) are improved by 3.97 and 3.4% in the counter-current mode compared with the co-current one.

Finally, it could be concluded that the thermally coupled double membrane reactor in the counter-current mode is an interesting candidate for production of pure hydrogen and methanol. However, from an industrial point of view there are still many issues to be addressed before putting a case for successful commercialization, such as: difficulties to construct a leak-free membrane reactor

with two sides, the catalysts would not age identically, the cost of membranes and it would require a situation where the quantities of the materials to be processed by the two reactions be in the proper balance.

Overall, operating and design parameters chosen for the reactor configuration lead to efficient coupling of the two reactions. The efficient coupling of the exothermic and endothermic reactions in a single vessel reduces the thermal losses associated with the supply of heat for the energy intensive endothermic process.

### Influence of Inlet Temperature of Endothermic Stream

The influence of the inlet temperature of the endothermic stream on the temperature profiles in the exothermic and endothermic sides along the reactor length for the counter-current mode is shown in Figure 6. As can be seen in Figure 6(a), increasing the inlet temperature of the endothermic stream leads to an increase of the exothermic side temperature in the first half of the reactor due to the pre-heating of the exothermic stream and afterwards, leads to a decrease in the temperature which is mainly due to more fuel depletion. Regarding to using non- and similar feed temperatures for the

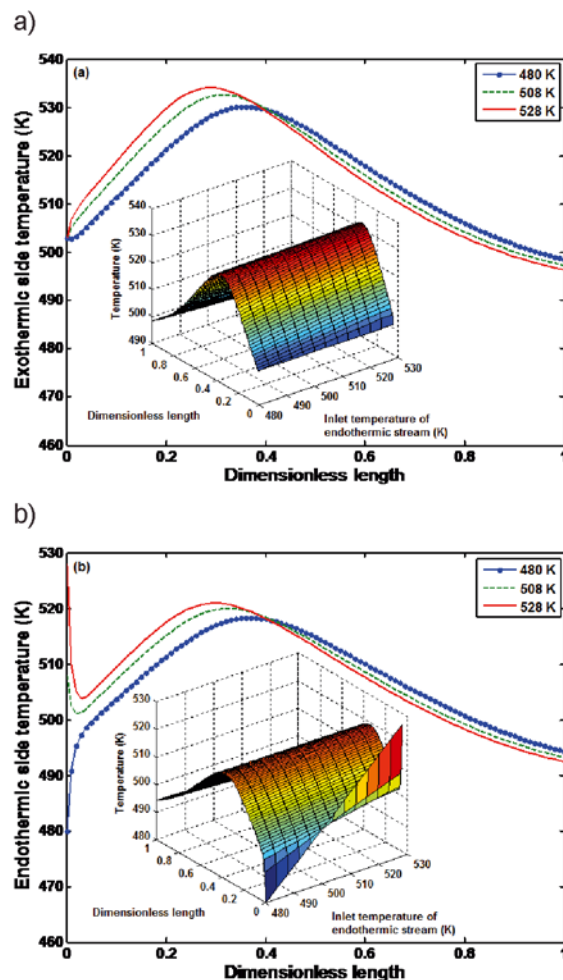


Figure 6. Influence of the inlet temperature of the endothermic stream on the temperature profiles in (a) exothermic and (b) endothermic sides along the reactor length for the counter-current configuration

Table 3. Comparison of different operation modes of ADMR performance

Operation mode	Conversion [%]		Yield		
	synthesis gas	C <sub>6</sub> H <sub>12</sub>	CH <sub>3</sub> OH	C <sub>6</sub> H <sub>6</sub>	H <sub>2</sub> recovery
Co-current	21.31	90.65	0.3803	0.9065	2.66
Counter-current	21.82	93.84	0.3899	0.9384	2.77

exothermic and endothermic streams, there are different cases where the cold spot in the endothermic side is or is not observed. The presence or absence of cold spot may be attributed to reasons such as dissimilar reaction rates and heats of the exothermic and endothermic reactions. One way of eliminating this cold spot is the utilization of the dissimilar feed temperature for the exothermic and endothermic streams. This arrangement requires the pre-heating of the exothermic stream and that can be carried out by utilizing the sensible heat of the exothermic stream leaving the reactor.

Figure 7(a) and (b) show the effect of the inlet temperature of the endothermic stream on the products yield and feedstock conversion, respectively. With increasing the inlet temperature of the endothermic stream from 480 to 528 K, the methanol and hydrogen recovery yields; and syngas and cyclohexane conversions increase which is due to higher temperature at first parts of the reactor and consequently, higher rate of reaction.

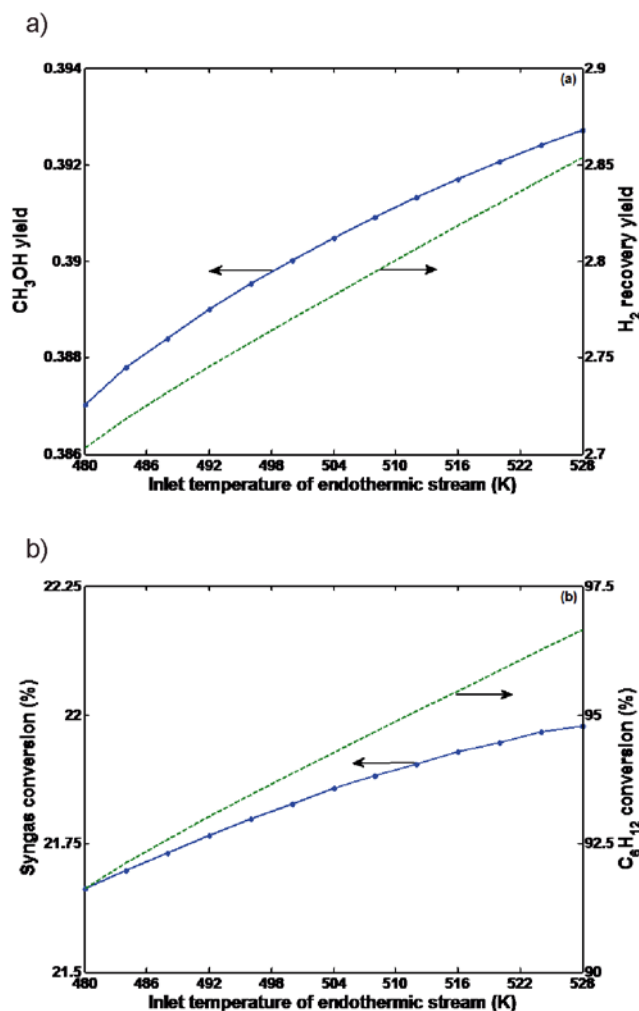


Figure 7. Influence of the inlet temperature of the endothermic stream on (a) methanol and hydrogen recovery yield and (b) syngas and cyclohexane conversions for the counter-current configuration

#### Influence of molar flow rate of endothermic stream

When the reactor geometry, inlet operating conditions and catalyst loading are fixed, variations of flow rates result in corresponding variations of fluid velocities and residence times. Figure 8(a) and (b) illustrate how the products yield and feedstock conversion behave along

the reactor axis when the flow rate of the endothermic stream increases from 0.1 to 0.3 mol s<sup>-1</sup>. As it can be seen in Figure 8(a), increasing the molar flow rate of the endothermic stream results in the reduction of the methanol and hydrogen recovery yield which is due to the decrease of synthesis gas and cyclohexane conversions (see Fig. 8(b)), respectively. By increasing the flow rate of the endothermic stream, axial exothermic temperature variation becomes lower which is due to higher transferred heat from the solid wall. As a result, the synthesis gas conversion decreases. Decrease of the cyclohexane conversion is an obvious consequence of the fact that the amount of catalyst in the endothermic side is not enough for these higher flow rates.

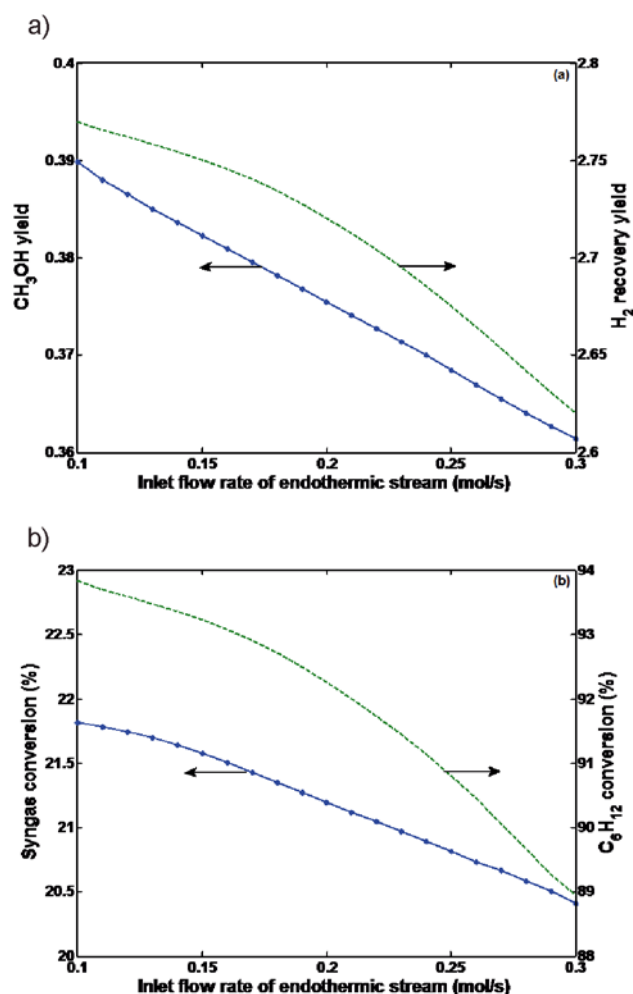


Figure 8. Influence of the molar flow rate of the endothermic stream on (a) methanol and hydrogen recovery yield and (b) syngas and cyclohexane conversions for the counter-current configuration

#### CONCLUSION

Simultaneous methanol and hydrogen production by the auto-thermal methanol synthesis process as well as hydrogen recovery have been studied using a one-dimensional steady-state model in a heat exchanger double-membrane reactor when two different hydrogen redistribution strategies are used in the recycle side. In the first strategy (the co-current configuration), the exothermic and recycle sides streams are in the co-current mode whereas in the second strategy (the counter-current configuration), the gas streams are in the reverse direction. The simulation results show that there

is a favorable profile of temperature in the exothermic side of the counter-current configuration and represent an enhancement in the methanol, hydrogen and benzene productivity in comparison with the co-current configuration. Besides, the counter-current mode is suitable from the environmental point of view due to lower carbon oxides emissions. The results suggest that utilization of the counter-current auto-thermal double-membrane reactor for pure hydrogen and methanol production could be feasible and beneficial. Experimental proof of the concept is needed to establish the validity and safe operation of the recuperative reactor.

## NOMENCLATURE

- $a_v$  – Specific surface area of catalyst pellet ( $\text{m}^2 \text{m}^{-3}$ )  
 $A_c$  – Cross section area of each tube ( $\text{m}^2$ )  
 $C_p$  – Specific heat of the gas at constant pressure ( $\text{J mol}^{-1}$ )  
 $D_i$  – Tube inside diameter (m)  
 $F$  – Total molar flow rate ( $\text{mol s}^{-1}$ )  
 $h_f$  – Gas-solid heat transfer coefficient ( $\text{W m}^{-2} \text{K}^{-1}$ )  
 $\Delta H_{f,i}$  – Enthalpy of formation of component  $i$  ( $\text{J mol}^{-1}$ )  
 $K$  – Rate constant of dehydrogenation reaction ( $\text{mol m}^{-3} \text{Pa}^{-1} \text{s}^{-1}$ )  
 $k_g$  – Mass transfer coefficient for component  $i$  ( $\text{m s}^{-1}$ )  
 $K_B$  – Adsorption equilibrium constant for benzene ( $\text{Pa}^{-1}$ )  
 $K_i$  – Adsorption equilibrium constant for component  $i$  in methanol synthesis reaction ( $\text{bar}^{-1}$ )  
 $K_p$  – Equilibrium constant for dehydrogenation reaction ( $\text{Pa}^3$ )  
 $K_{p,i}$  – Equilibrium constant based on partial pressure for component  $i$  in methanol synthesis reaction  
 $K_w$  – Thermal conductivity of reactor wall ( $\text{W m}^{-1} \text{K}^{-1}$ )  
 $L$  – Reactor length (m)  
 $N$  – Number of components ( $N = 6$  for methanol synthesis reaction,  $N = 3$  for dehydrogenation reaction)  
 $P_i$  – Partial pressure of component  $i$  (Pa)  
 $r_i$  – Reaction rate of component  $i$  (for exothermic reaction:  $\text{mol kg}^{-1} \text{s}^{-1}$ ; for endothermic reaction:  $\text{mol m}^{-3} \text{s}^{-1}$ )  
 $R$  – Universal gas constant ( $\text{J mol}^{-1} \text{K}^{-1}$ )  
 $T$  – Temperature (K)  
 $U$  – Overall heat transfer coefficient between exothermic and endothermic sides ( $\text{W m}^{-2} \text{K}^{-1}$ )  
 $y_i$  – Mole fraction of component  $i$  ( $\text{mol mol}^{-1}$ )  
 $Z$  – Axial reactor coordinate (m)

## Greek letters

- $\rho_b$  – Density of catalytic bed ( $\text{kg m}^{-3}$ )

## Superscripts

- G – In bulk gas phase  
 S – At surface catalyst

## LITERATURE CITED

1. Goltsov, V.A., Veziroglu, T.N. & Goltsova, L.F. (2006). Hydrogen civilization of the future – A new conception of the IAHE. *Int. J. Hydrogen Ener.* 31(2), 153–159. DOI: 10.1016/j.ijhydene.2005.04.045.

2. Ni, M., Leung, M.K.H., Leung, D.Y.C. & Sumathy, K. (2007). A review and recent developments in photocatalytic water-splitting using  $\text{TiO}_2$  for hydrogen production. *Renew. Sustain. Energy Rev.* 11(3), 401–425. DOI: 10.1016/j.rser.2005.01.009.

3. Ni, M., Leung, M.K.H., Sumathy, K. & Leung, D.Y.C. (2006). Potential of renewable hydrogen production for energy supply in Hong Kong. *Int. J. Hydrogen Energy* 31(10), 1401–1412. DOI: 10.1016/j.ijhydene.2005.11.005.

4. Ni, M., Leung, D.Y.C., Leung, M.K.H. & Sumathy, K. (2006). An overview of hydrogen production from biomass. *Fuel Process. Technol.* 87(5), 461–472. DOI: 10.1016/j.fuproc.2005.11.003.

5. Ye, G., Xie, D., Qiao, W., Grace, J.R. & Lim, C.J. (2009). Modeling of fluidized bed membrane reactors for hydrogen production from steam methane reforming with Aspen Plus. *Int. J. Hydrogen Energy* 34(11), 4755–4762. DOI: 10.1016/j.ijhydene.2009.03.047.

6. Biniwale, R.B., Kariya, N. & Ichikawa, M. (2005). Dehydrogenation of cyclohexane over Ni based catalysts supported on activated carbon using spray-pulsed reactor and enhancement in activity by addition of a small amount of Pt. *Catal. Lett.* 105(1–2), 83–87. DOI: 10.1007/s10562-005-8009-x

7. Pande, J.V., Shukla, A. & Biniwale, R.B. (2012). Catalytic dehydrogenation of cyclohexane over Ag-M/ACC catalysts for hydrogen supply. *Int. J. Hydrogen Energy* 37(8), 6756–6763. DOI: 10.1016/j.ijhydene.2012.01.069.

8. Koutsonikolas, D., Kaldis, S., Zaspalis, V.T. & Sakellariopoulos, G.P. (2012). Potential application of a microporous silica membrane reactor for cyclohexane dehydrogenation. *Int. J. Hydrogen Energy* 37(21), 16302–16307. DOI: 10.1016/j.ijhydene.2012.02.076.

9. Chinchin, G.C., Denny, P.J., Jennings, J.R., Spencer, M.S. & Waugh, K.C. (1988). Synthesis of methanol: Part 1. catalysts and kinetics. *Appl. Catal.* 36, 1–65. DOI: 10.1016/S0166-9834(00)80103-7.

10. Wang, F., Liu, Y., Gan, Y., Ding, W., Fang, W. & Yang, Y. (2013). Study on the modification of Cu-based catalysts with cupric silicate for methanol synthesis from synthesis gas. *Fuel Process. Technol.* 110, 190–196. DOI: 10.1016/j.fuproc.2012.12.012.

11. Lee, D.H. & Kim, T. (2013). Plasma-catalyst hybrid methanol-steam reforming for hydrogen production. *Int. J. Hydro. Energy* 38(14), 6039–6043. DOI: 10.1016/j.ijhydene.2012.12.132.

12. Khzouz, M., Wood, J., Pollet, B. & Bujalski, W. (2013). Characterization and activity test of commercial  $\text{Ni}/\text{Al}_2\text{O}_3$ ,  $\text{Cu}/\text{ZnO}/\text{Al}_2\text{O}_3$  and prepared  $\text{Ni-Cu}/\text{Al}_2\text{O}_3$  catalysts for hydrogen production from methane and methanol fuels. *Int. J. Hydro. Energy* 38(3), 1664–1675. DOI: 10.1016/j.ijhydene.2012.07.026.

13. Khademi, M.H., Setoodeh, P., Rahimpour, M.R. & Jahanmiri, A. (2009). Optimization of methanol synthesis and cyclohexane dehydrogenation in a thermally coupled reactor using differential evolution (DE) method. *Int. J. Hydro. Energy* 34(16), 6930–6944. DOI: 10.1016/j.ijhydene.2009.06.018.

14. Khademi, M.H., Jahanmiri, A. & Rahimpour, M.R. (2009). A novel configuration for hydrogen production from coupling of methanol and benzene synthesis in a hydrogen-permselective membrane reactor. *Int. J. Hydro. Energy* 34(12), 5091–5107. DOI: 10.1016/j.ijhydene.2009.04.007.

15. Khademi, M.H., Rahimpour, M.R. & Jahanmiri, A. (2010). Differential evolution (DE) strategy for optimization of hydrogen production, cyclohexane dehydrogenation and methanol synthesis in a hydrogen-permselective membrane thermally coupled reactor. *Int. J. Hydro. Energy* 35(5), 1936–1950. DOI: 10.1016/j.ijhydene.2009.12.080.

16. Rahmani, F., Haghighi, M., Estifae, P. & Rahimpour, M.R. (2012). A comparative study of two different membranes applied for auto-thermal methanol synthesis process. *J. Nat. Gas Sci. Engine.* 7, 60–74. DOI: 10.1016/j.jngse.2012.04.001.

17. Rahimpour, M.R., Bayat, M. & Rahmani, F. (2010). Enhancement of methanol production in a novel cascading fluidized-bed hydrogen permselective membrane methanol reactor. *Chem. Engine. J.* 157(2–3), 520–529. DOI: 10.1016/j.cej.2009.12.048.
18. Rahimpour, M.R., Rahmani, F., Bayat, M. & Pourazadi, E. (2011). Enhancement of simultaneous hydrogen production and methanol synthesis in thermally coupled double-membrane reactor. *Int. J. Hydro. Energy*, 36(1), 284–298. DOI: 10.1016/j.ijhydene.2010.09.074.
19. Gallucci, F., Comite, A., Capannelli, G. & Basile, A. (2006). Steam reforming of methane in a membrane reactor: an industrial case study. *Industrial & Engine. Chem. Res.* 45(9), 2994–3000. DOI: 10.1021/ie058063j.
20. Gallucci, F., Basile, A., Tosti, S., Iulianelli, A. & Drioli, E. (2007). Methanol and ethanol steam reforming in membrane reactors: An experimental study. *Int. J. Hydro. Energy* 32(9), 1201–1210. DOI: 10.1016/j.ijhydene.2006.11.019.
21. Gallucci, F. & Basile, A. (2006). Co-current and counter-current modes for methanol steam reforming membrane reactor. *Int. J. Hydro. Energy* 31(15), 2243–2249. DOI: 10.1016/j.ijhydene.2006.05.007.
22. Gallucci, F., Paturzo, L. & Basile, A. (2004). Hydrogen recovery from methanol steam reforming in a dense membrane reactor: simulation study. *Industrial & Engine. Chem. Res.* 43(10), 2420–2432. DOI: 10.1021/ie0304863.
23. Chen, Z., Yan, Y. & Elnashaie, S.S.E.H. (2003). Non-monotonic behavior of hydrogen production from higher hydrocarbon steam reforming in a circulating fast fluidized bed membrane reformer. *Industrial & Engine. Chem. Res.* 42(25), 6549–6558. DOI: 10.1021/ie021013j.
24. Basile, A., Paturzo, L. & Gallucci, F. (2003). Co-current and counter-current modes for water gas shift membrane reactor. *Catal. Today* 82(1–4), 275–281. DOI: 10.1016/S0920-5861(03)00241-4
25. Rahimpour, M.R., Moghtaderi, B., Jahanmiri, A. & Rezaie, N. (2005). Operability of an industrial methanol synthesis reactor with mixtures of fresh and partially deactivated catalyst. *Chem. Engine. & Technol.* 28(2), 226–234. DOI: 10.1002/ceat.200407062.
26. Rezaie, N., Jahanmiri, A., Moghtaderi, B. & Rahimpour, M.R. (2005). A comparison of homogeneous and heterogeneous dynamic models for industrial methanol reactors in the presence of catalyst deactivation. *Chem. Engine. Proces.* 44(8), 911–921. DOI: 10.1016/j.cep.2004.10.004.
27. Graaf, G.H., Scholtens, H., Stamhuis, E.J. & Beenackers, A.A.C.M. (1990). Intra-particle diffusion limitations in low-pressure methanol synthesis. *Chem. Engine. Sci.* 45(4), 773–783. DOI: 10.1016/0009-2509(90)85001-t.
28. Graaf, G.H., Sijtsema, P.J.J.M., Stamhuis, E.J. & Joosten, G.E.H. (1986). Chemical equilibria in methanol synthesis. *Chem. Engine. Sci.* 41(11), 2883–2890. DOI: 10.1016/0009-2509(86)80019-7.
29. Itoh, N. (1987). A membrane reactor using palladium. *AIChE J.* 33(9), 1576–1578. DOI: 10.1002/aic.690330921.
30. Jeong, B.H., Sotowa, K.I. & Kusakabe, K. (2003). Catalytic dehydrogenation of cyclohexane in an FAU-type zeolite membrane reactor. *J. Mem. Sci.* 224(1–2), 151–158. DOI: 10.1016/j.memsci.2003.08.004.
31. Rahimpour, M.R. & Ghader, S. (2003). Theoretical investigation of a Pd-membrane reactor for methanol synthesis. *Chem. Engine. & Technol.* 26(8), 902–907. DOI: 10.1002/ceat.200301717.
32. Reid, R.C. & Sherwood, T.K. (1969). *The properties of gases and liquids* (Second Edition ed.). New York: McGraw-Hill.
33. Lindsay, A.L. & Bromley, L.A. (1950). Thermal conductivity of gas mixture. *Industrial & Engine. Chem. Res.* 42(8), 1508–1511. DOI: 10.1021/ie50488a017.
34. Cussler, E.L. (2009). *Diffusion: mass transfer in fluid systems* (3rd ed.): Cambridge University Press.
35. Rahimpour, M.R. & Pourazadi, E. (2011). A comparison of hydrogen and methanol production in a thermally coupled membrane reactor for co-current and counter-current flows. *Int. J. Energy Res.* 35(10), 863–882. DOI: 10.1002/er.1744.